Published in final edited form as:
J Control Release. 2010 April 2; 143(1): 13–22. doi:10.1016/j.jconrel.2009.12.010.

An optical and microPET assessment of thermally-sensitive liposome biodistribution in the Met-1 tumor model: importance of formulation

E. E. Paoli[a], **D. E. Kruse**[a], **J. W. Seo**[a], **H. Zhang**[a], **A. Kheirolomoom**[a], **K. D. Watson**[a], **P. Chiu**[b], **H. Stahlberg**[b,†], and **K. W. Ferrara**[a,*]

[a] Department of Biomedical Engineering, University of California, Davis, CA 95616, USA

[b] Department of Molecular and Cellular Biology, University of California, Davis, CA 95616, USA

Introduction

There is great momentum for image-guided interventions (IGI) in general and image-guided drug delivery (IGDD) in particular, with many activatable particles under development [1–8]. Encapsulating chemotherapeutics within liposomes significantly reduces the toxicity of those drugs [9–11]. Unfortunately, the protective coating of liposomes reduces drug diffusion within the tumor [12]. Therefore, activation of particles at the disease site is of interest. Preclinical and clinical studies of activatable drug delivery vehicles are expanding [1,2,13–18]. Temperature-sensitive liposomes encapsulating doxorubicin (Thermodox, Celsion, MD) are under evaluation for the treatment of liver and breast cancer, generally using microwave radiation as a heat source [19]. The Thermodox formulation releases at a clinically-desirable temperature of ~39°C due to the incorporation of a lysolipid to decrease the phase transition temperature of the particle; this incorporation also enhances the ion permeability and drug release rates at the membrane phase transition [20].

In order to reliably activate the particle in the region of interest, the development of imaging methods to track the particle is required. Image guidance methods using magnetic resonance imaging, ultrasound, and X-Ray computed tomography are well-known [21–24]; however, image-guidance using nuclear medicine techniques are attractive due to their high sensitivity. Radioactive labeling of nanoparticles for use in single photon emission computed tomography (SPECT) has been frequently reported, but positron emission tomography (PET) has substantial advantages in sensitivity and spatial resolution. We have developed methods for labeling liposomes or other nanoparticles for PET imaging [17,25], and we employ these methods to evaluate the stability and accumulation of the particle shell. Similarly, many probes have been incorporated within particles for *in vitro* studies of the loading and release of drugs [26–28]; however, here we uniquely encapsulate a quenched near-infrared fluorophore. Sensitive detection of release and accumulation of the model drug in specified ROIs by measuring superficial fluorescence is then used to design long circulating, yet activatable, particles.

*Corresponding author. Present address: University of California Davis, Department of Biomedical Engineering, Davis, CA 95616, USA. Tel.: +1-530-7549436; fax: +1-530-7545739; kwferrar@ucdavis.edu.
†present address: C-CINA, Biozentrum, University Basel, CH-4056 Basel, Switzerland

Using a hydrophilic model drug, our goal was to assess the relative stability and circulation kinetics, while maintaining temperature sensitivity. In order to engineer a stable formulation, we compare the stability of formulations with varied PEG coating, lysolipid content, cholesterol content, charge and osmolarity. Cholesterol has previously been shown to be important in the stabilization of liposomes to the effects of plasma [29]. Osmotically-shrunken liposomes are also of increasing interest for contrast agents in magnetic resonance imaging, due to chemical exchange saturation transfer (CEST) mechanisms [30]. In addition, we evaluate the use of PET and optical imaging for real-time evaluation of the pharmacokinetics of our particles. We summarize *in vitro* fluorophore release, *in vivo* circulation and measures of tumor accumulation. Comparing liposome circulation and tumor accumulation over 24 hours using both PET and optical methods aids in determining sources of liposome instability by monitoring of both the exterior lipid shell and the interior aqueous core.

By employing new imaging techniques, temperature sensitive vehicles with enhanced stability are validated. Both high cholesterol and low osmolarity formulations accumulate within a tumor at levels far greater than free drug. The systemic toxicity of chemotherapeutic drugs such as doxorubicin and cisplatin limits their use; a stable, yet activatable formulation would enhance efficacy while reducing off-target effects. The development of imaging techniques to screen vehicles for their stability and activation holds promise for vehicle engineering.

Materials and Methods

Fluorophores

Alexa Fluor 750 succinimidyl ester (AF-750) was purchased from Invitrogen (Carlsbad, CA). An aqueous solution of AF-750 (2.5 mM) was created by dissolving AF-750 directly into a buffer of the desired osmolarity (10–300 mOsm) which was adjusted by diluting 1x PBS with diH_2O. Prior to use, the aqueous solution of AF-750 was heated at 50°C for 30 minutes and incubated overnight at room temperature to ensure complete hydrolysis the succinimidyl ester. For the *in vivo* studies, the AF-750 probe encapsulated within the particles was significantly quenched when loaded at a concentration above 1 mM while providing sufficient signal for optical imaging (Supplementary Fig. 1a) and therefore the internal concentration used in these studies was 2.5 mM. Using a partially quenched fluorophore provides an instantaneous indication of dye release due to the detectable increase in fluorescence with de-quenching, yet facilitates tracking of the circulating particles.

Calcein Bis[N,N−bis(carboxymethyl)aminomethyl]fluorescein was purchased from Sigma Chemical Co. (St. Louis, MO). A 50 mM aqueous solution was created by dissolving calcein in phosphate buffer which was adjusted with NaOH to obtain a pH of 7.45 and the desired osmolarity of 300 mOsm.

Lipids

1,2-Dipalmitoyl-sn-Glycero-3-Phosphatidylcholine (DPPC), 1,2-Distearoyl-sn-Glycero-3-Phosphoethanolamine-N-[Methoxy (Polyethylene glycol)-2000] (DSPE-PEG2k), 1,2-Distearoyl-sn-Glycero-3-Phosphatidylcholine (DSPC), N-Palmitoyl-Sphingosine-1-[Succinyl (methoxypolyethyleneglycol) 2000] (Ceramide-PEG2k), L-α-Phosphatidylcholine (hydrogenated-SoyPC), Cholesterol (Chol), and 1-Palmitoyl-2-Hydroxy-sn-Glycero-3-Phosphatidylcholine (lyso-PalmitoylPC) were purchased from Avanti Polar Lipids (Alabaster, AL) and stored at −20°C in chloroform. Distearoylphosphatidylethanolamine copolymer of polyoxyethylene monoallyl monomethyl ether and maleic anhydride “DSPE-AM0530K” (Comb-PEG) was purchased from NOF Corporation (Tokyo, Japan) and stored at −20°C in chloroform.

Preparation of Fluorescent Liposomes

Liposomes were prepared by the lipid film hydration and extrusion method [31]. Briefly, lipids dissolved in chloroform were mixed at the molar ratios shown in Table 1, dried into a thin film under a gentle stream of nitrogen and subsequently placed under vacuum overnight. The dried lipid film was rehydrated in the desired fluorophore solution to create a lipid concentration of 50 mg/ml and warmed at 55°C for 50 minutes with gentle vortexing every 10 minutes. The resultant multilamellar lipid vesicles were extruded through a 100 nm polycarbonate filter at a temperature ~10°C above the liposomal phase transition temperature. The unencapsulated fluorophore (calcein or AF-750) was then separated from the liposome vesicles by gel filtration using Sephadex G-75 (GE Healthcare, Sweden) and collected to a final lipid concentration of 3 mg/ml. The mean diameter of the liposomes (100 ± 20nm) was verified using a NICOMP submicron particle analyzer (NICOMP 380, Particle Sizing Systems Inc., Santa Barbara, CA, USA). Each formulation was matched for both lipid and dye concentration during vesicle formation and validated by measuring lipid concentration with a phospholipid assay (Wako Chemicals USA, Inc., Richmond, VA) and measuring fluorescence following vesicle rupture with a Triton X-100 solution.

Detection of Release *in vitro*

The self-quenching property of calcein at a concentration of 50 mM was used to monitor liposome dye retention in both buffer and mouse serum at 37°C and 42°C over 90 min in a plate reader (model FLx800, BioTek Instruments, Inc., Winooski, VT) using 493 nm as an excitation wavelength and 513 nm as an emission wavelength [32]. The percent fluorophore release was determined using the following formula: $[(I_x - I_i)/(I_d - I_i)] \times 100$, where I_x was the measured intensity at time x, I_d was the signal measured after liposome destruction, and I_i was the measured initial fluorescence. Using a fluorimeter to measure intensity changes over time, calcein release kinetics were quantified. To ensure precise temperature release profiles, 2 mL of either PBS or mouse serum was pre-warmed to the desired temperature before 50 μL of room temperature liposome suspension (3 mg/ml) was added. The addition of 50 μL of room temperature liposomes did not measurably change the temperature of the pre-warmed 2ml of PBS or mouse serum in which the tests were being preformed, thus effectively eliminating any heat ramping effects. To determine I_i, the initial fluoresce prior to dye release, 50 μL of liposome suspension (3 mg/ml) was mixed with 2mL of PBS or mouse serum. To determine I_d, the intensity of 100% release, 50 μL of liposome suspension (3 mg/ml) was mixed with 2 μL of 10% Triton X-100, vortexed, and heated at 55°C for 5 min. Next, PBS or mouse serum (Innovative Research, Inc., Novi, MI) was added to this solution to precisely match the liposome concentration, in which the heating experiments were performed and the fluorescence intensity measured. This indirect method of releasing encapsulated dye was performed since complete dye release was not always possible when liposomes were first mixed in mouse serum before adding the Triton X-100 solution. All fluorescence measurements were performed after allowing samples to reach 22°C (room temperature).

Temperature stability and release experiments were then performed using AF-750 to measure liposome dye retention in both buffer and mouse serum at 37°C and 42°C over 90 min. AF-750 is an ideal probe for near infrared *in vivo* imaging, whereas calcein is superior for rapid *in vitro* studies as dye release can be directly quantified without further purification. Unlike highly quenchable calcein, AF-750, with its relatively small ratio of quenched to unquenched intensity, must be purified following liposomal release prior to measurement. Released AF-750 was separated from encapsulated AF-750 using Centrisart 10,000 MW cut off spin filter columns (Sartorius Stedim Biotech, Goettingen, Germany) for accurate fluorophore quantification. The concentration of free AF-750 was measured with an excitation wavelength of 750 nm and an emission wavelength of 800 nm.

Animal Model

Animals were maintained within a University of California, Davis vivarium and all procedures were approved by the UC Davis Committee on Animal Use and Care. Female FVB mice (Charles River Laboratories, Wilmington, MA) underwent transplantation of Met-1 tumor cells from donor mice [33,34]. One mm^3 pieces of the donor Met-1 tumor were bilaterally transplanted into the 4^{th} mammary fat pads of 3-week-old mice. Mice were imaged when transplanted tumors reached 0.5 cm in diameter on average, which required ~14 days post-transplantation. Twenty-four hours prior to imaging, fur was removed along the mid section of the mice.

In vivo Imaging

Live animal fluorescence optical imaging monitored the *in vivo* biodistribution of fluorescently-loaded liposomes using the IVIS Caliper system (Caliper Life Sciences Corp., Alameda, CA). Images were acquired and analyzed with Living Image software 2.5 (Caliper Life Sciences Corp.) with identical illumination settings for all images. The system settings were: binning = 4, exposure time = 5 seconds, field-of-View = 15, f-Stop = 2 and filters with an excitation of 705–780 nm and emission of 810–885 nm. Data are displayed in the unitless value of efficiency and represent the ratio of light emitted to light incident. Mice were sedated via inhalation of isoflurane/oxygen and injected with a volume of 150 μL of liposome solution via the tail vein.

Formulations were tested via injection of AF-750 loaded liposomes containing 450 μg of lipid and 1.5 nMol of AF-750. Each dose was matched for fluorophore and lipid concentration. *In vivo* images were acquired over 24 hours in four positions (ventral decubitus, right lateral decubitus, left lateral decubitus and dorsal decubitus) and fluorescence of major organs was differentiated. Clearance of the optical probe AF-750 was quantified by bladder fluorescence with the mouse imaged in dorsal decubitus, concentration of the fluorophore in the blood pool was estimated from the superficial tissue at the mid-back with the mouse imaged in ventral decubitus, and tumor fluorescence was estimated with the mouse imaged in the right and left lateral decubitus position. Twenty-four hours post-injection, *ex vivo* fluorescence images of dissected tissues were acquired and tissue was processed further with a cell-digest preparation and assayed for fluorescence.

A serial dilution of liposomes ranging from 45 to 180 μg lipid and 0.15 to 0.6 nMols AF-750 were injected into FVB mice via the tail vein to test the linearity of *in vivo* fluorescence efficiency for particles within the blood pool. Images were acquired immediately post injection to minimize any liposome clearance effects. The concentration of the fluorophore in the blood pool was estimated placing a region of interest around superficial tissue at the mid-back with mouse imaged in the ventral decubitus position.

PET images were separately acquired using both ^{18}F and ^{64}Cu labeled lipids to monitor *in vivo* biodistribution of the liposome bilayer. The ^{18}F and ^{64}Cu radiolabeled liposomes were prepared as described by Marik [25] and Seo [17], respectively.

Enzymatic Tissue Digestion

A tissue digestion buffer was modified from [35] and consisted of 100 mM Tris/HCl (pH 8.5), 1 mM EDTA, 0.5% sodium dodecyl sulfate, and 200 mM sodium chloride. Prior to tissue digestion, 0.1 U/mg of proteinase K was added. Tumors were manually sliced into 1 mm^3 cubes while frozen and mixed with the tissue digestion buffer at a ratio of 3 μL digestion buffer per 1 mg of tumor. Samples were incubated at 55°C for 3 hours while vortexing for 5 minutes once an hour.

Cryo-transmission electron microscopy

For cryo-transmission electron microscopy (cryo-EM) imaging, 3.5 μl of liposome suspensions at an approximate concentration of 1 mg/ml were adsorbed to glow-discharged holey carbon film-coated copper grids (Quantifoil Micro Tools, GmbH), blotted, and quick-frozen by plunging into liquid ethane slush, to obtain an unstained vitrified cryo-EM specimen [36]. Grids were transferred with a Gatan 626 cryo sample holder into a JEOL JEM-2100F transmission electron microscope operated at 200 kV. Images were recorded on a TVIPS F415 CCD camera at a nominal magnification of 50,000x, under minimum dose conditions.

Statistics

The mean and standard deviation of measurements was computed. For individual statistical comparisons between groups, two tailed Student's t-tests were performed to compare the means of the measured parameters. The Bonferroni correction was performed for multiple comparisons to maintain the global P value at 0.05; all values lower than 0.05 were considered significant. In addition, linear regression was performed on data sets to characterize apparent trends in the data. Nine groups of n=4 mice, each with bilateral tumors, were studied. Our PET and optical assessments of tumors demonstrate a 10% standard deviation. Therefore, n=4 was chosen to detect a 20% change between groups for two-sided tests with alpha=0.05 at a power of 0.8.

Results

For each particle, lipid and dye concentrations were matched, as reported in [43], with a goal of achieving a particle diameter of ~80–100 nm. The mean liposomal diameter observed was in all cases between 80 and 113 nm with an average standard deviation of ±20 nm.

In vitro stability and temperature response from liposomes

In vitro fluorescence was first evaluated in PBS (not shown) and mouse serum at temperatures of 37°C and 42°C (Fig. 1b and 1c). Incorporating high molar concentrations of cholesterol into the liposomal membrane decreased the calcein leakage rates at all temperatures tested (**I and II,** Fig. 1). Alternatively, the incorporation of lyso-palmitoylPC resulted in the loss of approximately 50% of the encapsulated calcein within 5 minutes of incubation in mouse serum at 37°C (**III and IV,** Fig. 1b), as also previously observed in [44]. However, this rapid release was not observed when incubating lyso-palmitoylPC formulations in PBS, all formulations released under 5% over 90 minutes (not shown). Formulations (II, V–IX) were stable at 37°C in serum, releasing less than 20% of the fluorophore over 90 minutes, while remaining temperature responsive when heated to 42°C (Fig. 1b and 1c). With an increase in the incubation temperature to 42°C, all formulations released more than 25% of their encapsulated fluorophore within the first 5 minutes with the exception of formulation I, which is not temperature sensitive (Fig. 1c). Similar trends were observed when calcein was replaced with AF-750; Formulation I released less than 3% over 90 minutes and Formulation III released more than 40% within 1 minute at 42°C (data not shown).

In vivo studies combining PET and optical imaging

In order to validate the linearity of *in vivo* optical imaging to quantify fluorophore concentration in the blood pool, AF-750-loaded liposomes were imaged immediately after injection of relevant concentrations of the highly stable Formulation I. Increasing the mass of injected AF-750-loaded liposomes from 45 to 180 μg lipid (and thus 0.15 to 0.6 nanomoles AF-750), led to a corresponding linear increase in detected fluorescence R^2 =0.994 (Fig. 2a).

To further validate our *in vivo* optical imaging methods, we then compared optical and PET images in tumors and the blood compartment for vehicles with very high and lesser stability. The AF-750 optical probe used in these studies clears rapidly when injected as a free dye (Supplementary Fig. 1b), facilitating its use as a marker of vehicle stability. A lipid conjugated with the 6-[p-(bromoacetamido)benzyl]- 1,4,8,11-tetraazacyclotetradecane-N,N',N'',N'''-tetraacetic acid (BAT) chelator was incorporated within the liposome at a low concentration (0.5 molar%) and the ^{64}Cu isotope was added and purified immediately before injection for studies over 24 hours. For studies of the circulation and metabolism of the lipid, an ^{18}F-labeled lipid was incorporated into the vehicle at the time of vehicle formation.

PET images of formulations I and III acquired during the initial 10 minutes post-injection and 60–70 minutes post-injection demonstrate that the lipid shell continues to circulate, with conspicuous radioactivity observed in the heart and carotid arteries (Fig 1d). An increase in the lipid metabolism was demonstrated by the increased bladder activity in formulation III, as compared with formulation I at the 60–70 minute time point (Fig 1d). The differences between the two formulations are accentuated in the optical images. PET and optical images of formulation I were nearly unchanged over the 70-minute interval post-injection. Conversely, for formulation III, the optical efficiency in superficial tissues was greater at the 70-minute time point (Fig 1d) and decreases over time (Fig 2b). The initial increase in fluorescence is expected as the fluorophore is unquenched when outside the vehicle, providing a sensitive indication of initial dye release.

PET imaging of an ^{18}F-labelled lipid over 6 hours demonstrated the extended circulation of cholesterol rich formulation I (as compared with formulation III, $p < 0.002$), with formulation I activity in the blood pool exceeding 37% ID at 6 hours (Fig. 2b and 2e). Activity of the radiolabeled lipid within the blood pool was then compared with the optical efficiency of the blood pool as represented by superficial tissues over six hours (Fig 2b). The high concentration of cholesterol and long acyl chain of formulation I resulted in stable circulation of both the lipid and aqueous core. For formulation I, optical efficiency in superficial tissues, as shown over 6 hours, was highly correlated with the PET estimate of radioactivity in the blood pool (R^2=0.95). The optical efficiency of formulation III (containing a lysolipid) decreased more rapidly than the corresponding lipid radioactivity (R^2=0.62), presumably due to fluorophore leakage (Fig. 2b). Accumulation within the tumor was assessed over 24 hours by both PET and optical methods with regression of the normalized values yielding R^2 values of 0.95 and 0.96, respectively (Fig. 2c). For formulation III, while the blood pool optical efficiency (from the loaded fluorophore) was not highly correlated with the PET-based kinetics of the shell, tumor kinetics of the fluorophore and shell were correlated with the greatest accumulation occurring at the early time points before separation of shell and core. Activity within the bladder at 1 hour after injection, as assessed from the imaging data, demonstrated significant accumulation of the fluorophore following injection of formulation III (Fig. 2d).

From the 6-hr and 48-hr biodistribution, the radioactivity in the blood pool was greater for formulation I as compared with formulation III ($p<0.002$) (Fig. 2e). The radioactivity in the urine was greater for formulation I at 48 hours corroborating prolonged fluorophore circulation ($p=0.034$) (Fig. 2e). Finally, from the 48-hr biodistribution, accumulation of the particles within the tumor was significantly greater with formulation I ($p<0.05$) (Fig. 2e).

Exploring liposomal formulations

The optical methods were then employed to study the pharmacokinetics of nine formulations in order to determine whether such optical methods would predict eventual tumor accumulation of the hydrophilic cargo. *Ex vivo* quantification of organ fluorescence 24-hours post intravenous injection was performed for the following tissues: heart, lungs, liver, tumors, kidneys, spleen and leg muscle. Long-circulating formulations (I, II and IX) demonstrated the

greatest fluorescence across all tissues with the highest fluorescence in the tumors, where the tumor signal was over 10 times that observed in muscle (Fig. 3a). Relative to AF-750 encapsulated in formulation I, less than 2% of free AF-750 accumulated within the tumor over 24 hours (Fig. 3a). Across the nine formulations, *in vivo* and *ex vivo* quantifications of tumor fluorescence using Living Image software were each proportional to the fluorescence normalized to the highest measured signal of the digested tumor measured *ex vivo* (Fig. 3b), R^2=0.96 and R^2=0.99, respectively.

Fluorophores initially encapsulated in liposome formulations I and II, composed of 39 and 16 molar % cholesterol, achieved the highest tumor accumulation of AF-750, 177 and 101 times greater than that of free dye, respectively, at 24 hours post-injection (Fig. 3c). Fluorophore tumor accumulation resulting from a cholesterol-free formulation was 29 fold to 66 fold greater than free dye as the osmolarity decreased from 300 to 10 mOsm (**VII and IX,** Fig. 3c). Accumulation of lysolipid-containing formulations was 2.6% of that measured with the cholesterol-rich formulation I, with no improvement observed with a net neutrally-charged PEG moiety (**III and IV,** Fig. 3c). However, by switching from DSPE-PEG to a neutral-PEG derivative (formulation VII), the efficiency achieved by this modified formulation in the tumor at 24 hours increased by 5 times (Fig. 3c). Tumor fluorescence increased between 12 and 24 hours only with cholesterol-rich formulation I; however, the increase was not significant (p=0.1). In all other formulations, tumor fluorescence decreased from 12 to 24 hours, with significant decreases observed in formulations III, IV, V, VI, VII and IX (p-values 0.037,0.036,1.4×10^{-5}, 6.0×10^{-4},5.8×10^{-3},0.042 respectively) (Fig. 3d).

Imaging-based pharmacokinetics

Real-time optical imaging shown in Fig. 4 from these same studies was then quantified and compared with the biodistribution data. Here, circulation of the optically-labeled particles was shown by the “blue” coloring of the superficial tissues, increasing globally to yellow or red in superficial tissues as a result of unquenching and increasing to yellow or red in the tumor or bladder due to accumulation. Fig. 4 shows three views of the circulating vehicles for a range of formulations containing the same dye and lipid concentration, where a set of views was acquired at each time point. Release of the dye from the vehicle was readily apparent from the initially increased fluorescence in superficial tissues (the dye was initially quenched). When the dye concentration falls further, the fluorescence decreases.

Optical image efficiency of superficial tissue following injection of AF-750 loaded liposomes was quantified and normalized by initial fluorescence for each formulation (Fig. 5). Free fluorophore (once released from the liposome) was cleared very rapidly from circulation; 70% cleared within the first hour of circulation (Supplementary Fig. 1b). The normalized optical efficiency for formulation I *in vivo* remained over 79% for 24 hours in superficial tissues (Fig. 5a). Likewise, formulation II showed similar stability with an optical efficiency over 70% during the first 12 hours (Fig. 5a). The *in vitro* instability observed for formulations III and IV (containing lysolipids) was mirrored *in vivo*, decreasing to optical efficiencies below 5% within the first 12 hours of circulation (Fig. 5b). Although formulation V did not release during *in vitro* incubation, the optical efficiency decreased rapidly after injection, with an optical efficiency below 9.5% after 12 hours in circulation (Fig. 5b).

In order to improve performance of the classical temperature sensitive liposome (formulation V), we investigated several modifications: the addition of comb-PEG, neutral-PEG and hypo-osmolarity; in each case the liposomes had both equal fluorophore and lipid concentrations. Changing the PEG moiety from DSPE-PEG (formulation V) to Comb-PEG (formulation VI) produced 6.5 times greater optical efficiency in superficial tissue at 12 hours ($p<3\times10^{-4}$) (Fig. 5a). Switching the PEG moiety in formulation V to a neutral-PEG derivative (formulation VII), the optical efficiency of superficial tissue increased from 27% to 66% for times up to 6 hours

after injection ($p<0.03$) (Fig. 5b). Hypo-osmotic loading had the greatest effect on increasing the optical efficiency at later time points. Decreasing the osmolarity of the liposomal aqueous core from 300 mOsm (formulation VII) to 30 mOsm (formulation VIII) increased the optical efficiencies at both 12 hours ($p<0.003$) and 24 hours ($p<0.004$). Decreasing the osmolarity from 30 mOsm to 10 mOsm (formulation IX) again increased the optical efficiencies at both 12 hours ($p<4\times10^{-5}$) and 24 hours ($p<5\times10^{-4}$) (Fig. 5c). The 10 mOsm hypotonic formulation (formulation IX) demonstrated greater bladder fluorescence at 24 hours after injection as compared to formulation VII ($p<0.024$) and formulation VIII ($p<0.013$), corroborating the prolonged liposome circulation (Fig. 5d). A flattened morphology was observed for formulations VIII–IX with cryo-electron microscopy; all cryo-electron microscopy was performed with liposomes suspended in a 300 mOsm solution of PBS (Fig. 5e and 5f).

Discussion

While *in vitro* stability tests are useful in early characterization of plasma stability, *in vivo* biodistribution studies are ultimately needed to optimize stable drug-carrier formulations. Hypotheses as to why *in vitro* and *in vivo* liposome stability differ include: lysolipid and short acyl chain lipid separate from the particle during circulation (binding to other components), lipases can decrease stability subsequent to complement binding, and macrophage uptake can impact circulation time. In order to improve circulation and stability, we evaluated enhanced PEG coating, the elimination of lysolipid, the incorporation of cholesterol, and the elimination of charge on the PEG-lipid. Here, PET and optical imaging were combined to monitor the *in vivo* biodistribution of both the liposome shell and the entrapped aqueous core. This combination of imaging modalities allows for the differentiation between two mechanisms by which drug clearance from encapsulated vehicles occurs *in vivo*: liposome clearance through the reticulo-endothelial system and direct clearance of the drug through the leakiness of an otherwise long circulating lipid shell. Following a characterization of the mechanism of liposomal instability, specific alterations can be proposed to improve drug circulation. In our studies, PET was used to estimate the concentration of circulating lipid, as well as the metabolism and elimination of the lipid bi-products; similarly, optical imaging facilitated an estimate of the stability of the cargo within the vehicle. While planar optical imaging is not fully quantitative, our estimates of optical efficiency of a very bright near infrared fluorophore within tumors were highly correlated between *in vivo* and *ex vivo* studies, facilitating high-throughput measurements. Further, optical imaging of superficial tissue using a self-quenched fluorophore facilitated immediate visualization of fluorophore release. PET imaging of the shell and optical images of the core were highly correlated for a stable vehicle, but differ for an unstable vehicle. Future efforts will focus on the development of a pharmacokinetic model to characterize the circulation, elimination and stability of these particles.

We recognize that the permeability of each drug through a liposomal or polymer carrier is unique, and thus, carriers must ultimately be tested with the individual drug. However, there is a vast parameter space of vehicle chemistries, surface architecture, molecular targeting ligands and exogenous energy sources; successful optimization of the particle would be facilitated by the development of imaging methods to assess stability and release from the carrier for well-characterized model drugs. The immense importance of characterizing liposomal drug release kinetics in relation to enhanced therapeutic activity has been demonstrated in the murine breast cancer model [46]. The fluorophore used in our studies has a similar octanol:water partition coefficient to cisplatin (−2.3) and free fluorophore (and cisplatin) quickly clear from circulation with low tumor accumulation. Based on comparisons to Woo et al. [47], the plasma concentration of cisplatin decreased at a similar rate as the efficiency of our optical probe for formulations I, III, and V loaded with cisplatin. Further, our preliminary pharmacokinetic data for cisplatin loaded into formulations I and III (data not shown) are nearly identical to the results presented here for the model drug AF-750. Although

the accumulation of cisplatin is enhanced with encapsulation, liposomal vehicles containing cisplatin have not been efficacious [5,48–50]. Thus, this optical probe may facilitate a high-throughput initial screening of strategies for encapsulated cisplatin vehicles and strategies for enhanced release.

Rationalizations as to the differences noted between *in vitro* and *in vivo* release kinetics for those formulations demonstrating short circulation *in vivo* yet stable *in vitro* serum incubation were not further scrutinized in this study. Additional studies to investigate these differences and a potential connection to *in vivo* complement binding are underway.

While not shown, the imaging methods employed here can also be applied to assess the release of the drug from the carrier by exogenous energy. Here, we use formulation I as a gold standard for long circulation; however, the drug cannot be released from these vehicles with mild hyperthermia. Formulations (II and IX) were long circulating *in vivo* and temperature sensitive at 42°C and appear to be good starting points for the development of stable temperature-sensitive vehicles.

The use of a net neutrally-charged lipopolymer (Ceramide-PEG2k in formulations IV and VII) rather than the net negatively-charged lipopolymer (DSPE-PEG2k) did not significantly increase circulation time in this study. Vehicles containing lyso-PalmitoylPC circulated for a substantially shorter time interval than other formulations, with elimination of the lipid and the cargo observed within a few hours.

Decreasing the osmolarity of the buffer within which the drug was suspended (below 300 mOsm) improved liposomal fluorophore circulation. Electron microscopy of these particles demonstrated a flattened appearance at the time of injection, compared with the spherical shape of other formulations. Quantitation of the drug concentration as a function of time indicated that the particle was long circulating with a concentration of fluorophore in harvested tumors that was 66-fold higher than free drug and ~38% of that of formulation I (which is not temperature sensitive).

Conclusion

We conclude that combining PET and optical imaging is useful in the assessment and design of temperature-sensitive vehicles. Optical imaging of the dynamics of the liposome's aqueous core facilitates the design of temperature-sensitive formulations which circulate stably *in vivo*. Tumor accumulation of a model drug using a low-cholesterol (formulation II) and low-osmolarity (formulation IX) temperature-sensitive vehicle was 101 and 66-fold greater, respectively, than free fluorophore at 24 hours after injection; accumulation of a long-circulating cholesterol-rich formulation was 177-fold higher.

Supplementary Material

Refer to Web version on PubMed Central for supplementary material.

Acknowledgments

The support of NIH CA 103828 and NIH U54GM073929 is gratefully acknowledged.

References

1. Ponce AM, Viglianti BL, Yu DH, Yarmolenko PS, Michelich CR, Woo J, Bally MB, Dewhirst MW. Magnetic resonance imaging of temperature-sensitive liposome release: drug dose painting and antitumor effects. Journal of the National Cancer Institute 2007;99(1):53–63. [PubMed: 17202113]

2. Dromi S, Frenkel V, Luk A, Traughber B, Angstadt M, Bur M, Poff J, Xie JW, Libutti SK, Li KCP, Wood BJ. Pulsed-high intensity focused ultrasound and low temperature sensitive liposomes for enhanced targeted drug delivery and antitumor effect. Clinical Cancer Research 2007;13(9):2722–2727. [PubMed: 17473205]

3. Derfus AM, von Maltzahn G, Harris TJ, Duza T, Vecchio KS, Ruoslahti E, Bhatia SN. Remotely triggered release from magnetic nanoparticles. Advanced Materials 2007;19(22):3932–3936.

4. Gannon CJ, Patra CR, Bhattacharya R, Mukherjee P, Curley SA. Intracellular gold nanoparticles enhance non-invasive radiofrequency thermal destruction of human gastrointestinal cancer cells. Journal of Nanobiotechnology 2008;6 Article No.: 2.

5. Schroeder A, Honen R, Turjeman K, Gabizon A, Kost J, Barenholz Y. Ultrasound triggered release of cisplatin from liposomes in murine tumors. Journal of Controlled Release 2009;137(1):63–68. [PubMed: 19303426]

6. Kim IY, Kang YS, Lee DS, Park HJ, Choi EK, Oh YK, Son HJ, Kim JS. Antitumor activity of EGFR targeted pH-sensitive immunoliposomes encapsulating gemcitabine in A549 xenograft nude mice. Journal of Controlled Release 2009;140(1):55–60. [PubMed: 19616596]

7. Pradhan P, Giri J, Rieken F, Koch C, Mykhaylyk O, Döblinger M, Banerjee R, Bahadur D, Plank C. Targeted temperature sensitive magnetic liposomes for thermo-chemotherapy. Journal of Controlled Release. In Press, Corrected Proof.

8. Dewhirst MW, Vujaskovic Z, Jones E, Thrall D. Re-setting the biologic rationale for thermal therapy. International Journal of Hyperthermia 2005;21(8):779–790. [PubMed: 16338861]

9. Safra T, Muggia F, Jeffers S, Tsao-Wei DD, Groshen S, Lyass O, Henderson R, Berry G, Gabizon A. Pegylated liposomal doxorubicin (doxil): Reduced clinical cardiotoxicity in patients reaching or exceeding cumulative doses of 500 mg/m(2). Annals of Oncology 2000;11(8):1029–1033. [PubMed: 11038041]

10. Yildirim Y, Gultekin E, Avci ME, Inal MM, Yunus S, Tinar S. Cardiac safety profile of pegylated liposomal doxorubicin reaching or exceeding lifetime cumulative doses of 550 mg/m(2) in patients with recurrent ovarian and peritoneal cancer. International Journal of Gynecological Cancer 2008;18 (2):223–227. [PubMed: 17511800]

11. Olson F, Mayhew E, Maslow D, Rustum Y, Szoka F. Characterization, toxicity and therapeutic efficacy of adriamycin encapsulated in liposomes. European Journal of Cancer & Clinical Oncology 1982;18(2):167–169.

12. Kong G, Anyarambhatla G, Petros WP, Braun RD, Colvin OM, Needham D, Dewhirst MW. Efficacy of liposomes and hyperthermia in a human tumor xenograft model: importance of triggered drug release. Cancer Res 2000;60(24):6950–6957. [PubMed: 11156395]

13. Choi SH, Lee SH, Park TG. Temperature-sensitive pluronic/poly(ethylenimine) nanocapsules for thermally triggered disruption of intracellular endosomal compartment. Biomacromolecules 2006;7 (6):1864–1870. [PubMed: 16768408]

14. Han HD, Choi MS, Hwang T, Song CK, Seong H, Kim TW, Choi HS, Shin BC. Hyperthermia-induced antitumor activity of thermosensitive polymer modified temperature-sensitive liposomes. Journal of Pharmaceutical Sciences 2006;95(9):1909–1917. [PubMed: 16795016]

15. Hauck ML, Larue SM, Petros WP, Poulson JM, Yu DH, Spasojevic I, Pruitt AF, Klein A, Case B, Thrall DE, Needha D, Dewhirst MW. Phase I trial of doxorubicin-containing low temperature sensitive liposomes in spontaneous canine tumors. Clinical Cancer Research 2006;12(13):4004–4010. [PubMed: 16818699]

16. Schmaljohann D. Thermo- and pH-responsive polymers in drug delivery. Advanced Drug Delivery Reviews 2006;58(15):1655–1670. [PubMed: 17125884]

17. Seo JW, Zhang H, Kukis DL, Meares CF, Ferrara KW. A novel method to label preformed liposomes with 64Cu for positron emission tomography (PET) Imaging. Bioconjugate Chemistry 2008;19(12): 2577–2584. [PubMed: 18991368]

18. Shim WS, Kim JH, Kim K, Kim YS, Park RW, Kim IS, Kwon IC, Lee DS. pH- and temperature-sensitive, injectable, biodegradable block copolymer hydrogels as carriers for paclitaxel. International Journal of Pharmaceutics 2007;331(1):11–18. [PubMed: 17049773]

19. http://www.traxtal.com/home.html.

20. Mills JK, Needham D. Lysolipid incorporation in dipalmitoylphosphatidylcholine bilayer membranes enhances the ion permeability and drug release rates at the membrane phase transition. Biochimica Et Biophysica Acta -- Biomembranes 2005;1716(2):77–96.
21. Lencioni R, Crocetti L. Image-guided thermal ablation of hepatocellular carcinoma. Critical Reviews in Oncology/Hematology 2008;66(3):200–207. [PubMed: 18304832]
22. Chen X, Barkauskas KJ, Weinberg BD, Duerk JL, Abdul-Karim FW, Paul S, Saidel GM. Dynamics of MRI-guided thermal ablation of VX2 tumor in paraspinal muscle of rabbits. Ieee Transactions on Biomedical Engineering 2008;55:1004–1014. [PubMed: 18334392]
23. Yap JT, Carney JPJ, Hall NC, Townsend DW. Image-guided cancer therapy using PET/CT. Cancer Journal 2004;10(4):221–233.
24. Bale R, Widmann G. Navigated CT-guided interventions. Minimally Invasive Therapy & Allied Technologies 2007;16(4):196–204. [PubMed: 17763092]
25. Marik J, Tartis MS, Zhang H, Fung JY, Kheirolomoom A, Sutcliffe JL, Ferrara KW. Long-circulating liposomes radiolabeled with [F-18]fluorodipalmitin ([F-18]FDP). Nuclear Medicine and Biology 2007;34(2):165–171. [PubMed: 17307124]
26. Heyes J, Hall K, Tailor V, Lenz R, MacLachlan I. Synthesis and characterization of novel poly (ethylene glycol)-lipid conjugates suitable for use in drug delivery. Journal of Controlled Release 2006;112(2):280–290. [PubMed: 16603272]
27. Drummond DC, Noble CO, Guo ZX, Hong K, Park JW, Kirpotin DB. Development of a highly active nanoliposomal irinotecan using a novel intraliposomal stabilization strategy. Cancer Research 2006;66(6):3271–3277. [PubMed: 16540680]
28. Lee RJ, Low PS. Folate-targeted liposomes for drug delivery. Journal of Liposome Research 1997;7 (4):455–466.
29. Allen TM, Cleland LG. Serum-induced leakage of liposome contents. Biochimica Et Biophysica Acta 1980;597(2):418–426. [PubMed: 7370258]
30. Terreno E, Cabella C, Carrera C, Castelli DD, Mazzon R, Rollet S, Stancanello J, Visigalli M, Aime S. From spherical to osmotically shrunken paramagnetic liposomes: an improved generation of LIPOCEST MRI agents with highly shifted water protons. Angewandte Chemie-International Edition 2007;46(6):966–968.
31. Hope MJ, Bally MB, Webb G, Cullis PR. Production of large unilamellar vesicles by a rapid extrusion procedure. characterization of size, trapped volume and ability to maintain a membrane potential. Biochimica Et Biophysica Acta -- Biomembranes 1985;812(1):55–65.
32. Gregoriadis, G. Liposome technology. CRC Press; Boca Raton, Fla: 1984.
33. Wang L, Yao Q, Wang J, Wei GQ, Li GQ, Li D, Ling R, Chen JH. MRI and hybrid PET/CT for monitoring tumour metastasis in a metastatic breast cancer model in rabbit. Nuclear Medicine Communications 2008;29(2):137–143. [PubMed: 18094635]
34. Guy CT, Cardiff RD, Muller WJ. Induction of mammary-tumors by expression of polyomavirus middle T-oncogene - a transgenic mouse model for metastatic disease. Molecular and Cellular Biology 1992;12(3):954–961. [PubMed: 1312220]
35. Yu C, Penn LD, Hollembaek J, Li WL, Cohen LH. Enzymatic tissue digestion as an alternative sample preparation approach for quantitative analysis using liquid chromatography-tandem mass spectrometry. Analytical Chemistry 2004;76(6):1761–1767. [PubMed: 15018580]
36. Dubochet J, Adrian M, Chang JJ, Homo JC, Lepault J, McDowall AW, Schultz P. Cryo-electron microscopy of vitrified specimens. Quart Rev Biophys 1988;21:129–228.
37. Working PK, Dayan AD. Pharmacological-toxicological expert report - caelyx(TM) - (stealth(R) liposomal doxorubicin HCl) - foreword. Human & Experimental Toxicology 1996;15(9):751–785. [PubMed: 8880211]
38. Gaber MH, Hong KL, Huang SK, Papahadjopoulos D. Thermosensitive sterically stabilized liposomes - formulation and in-vitro studies on mechanism of doxorubicin release by bovine serum and human plasma. Pharmaceutical Research 1995;12(10):1407–1416. [PubMed: 8584472]
39. Needham D, Anyarambhatla G, Kong G, Dewhirst MW. A new temperature-sensitive liposome for use with mild hyperthermia: characterization and testing in a human tumor xenograft model. Cancer Research 2000;60(5):1197–1201. [PubMed: 10728674]

40. Webb MS, Saxon D, Wong FMP, Lim HJ, Wang Z, Bally MB, Choi LSL, Cullis PR, Mayer LD. Comparison of different hydrophobic anchors conjugated to poly(ethylene glycol): effects on the pharmacokinetics of liposomal vincristine. Biochim Biophys Acta-Biomembr 1998;1372(2):272–282.
41. Yatvin MB, Weinstein JN, Dennis WH, Blumenthal R. Design of liposomes for enhanced local release of drugs by hyperthermia. Science 1978;202(4374):1290–1293. [PubMed: 364652]
42. Matsumura S, Sato S, Yudasaka M, Tomida A, Tsruruo T, Iijima S, Shiba K. Prevention of carbon nanohorn agglomeration using a conjugate composed of comb-shaped polyethylene glycol and a peptide aptamer. Molecular Pharmaceutics 2009;6(2):441–447. [PubMed: 19718797]
43. Zhang H, Kusunose J, Kheirolomoom A, Seo JW, Qi J, Watson K, Lindfors H, Ruoslahti E, Sutcliffe JL, Ferrara KW. Dynamic imaging of arginine-rich heart-targeted vehicles in a mouse model. Biomaterials 2008;29(12):1976–1988. [PubMed: 18255141]
44. Hossann M, Wiggenhorn M, Schwerdt A, Wachholz K, Teichert N, Eibl H, Issels RD, Lindner LH. In vitro stability and content release properties of phosphatidylglyceroglycerol containing thermosensitive liposomes. Biochim Biophys Acta-Biomembr 2007;1768(10):2491–2499.
45. Qin S, Seo JW, Zhang H, Qi J, Curry F-RE, Ferrara KW. An imaging-driven model for liposomal stability and circulation. Molecular Pharmaceutics. (In Press, Accepted Manuscript).
46. Charrois GJR, Allen TM. Drug release rate influences the pharmacokinetics, biodistribution, therapeutic activity, and toxicity of pegylated liposomal doxorubicin formulations in murine breast cancer. Biochim Biophys Acta-Biomembr 2004;1663(1–2):167–177.
47. Woo J, Chiu GNC, Karlsson G, Wasan E, Ickenstein L, Edwards K, Bally MB. Use of a passive equilibration methodology to encapsulate cisplatin into preformed thermo sensitive liposomes. International Journal of Pharmaceutics 2008;349(1–2):38–46. [PubMed: 17728083]
48. Drummond DC, Noble CO, Hayes ME, Park JW, Kirpotin DB. Pharmacokinetics and In Vivo Drug Release Rates in Liposomal Nanocarrier Development. Journal of Pharmaceutical Sciences 2008;97 (11):4696–4740. [PubMed: 18351638]
49. Abu-Lila A, Suzuki T, Doi Y, Ishida T, Kiwada H. Oxaliplatin targeting to angiogenic vessels by PEGylated cationic liposomes suppresses the angiogenesis in a dorsal air sac mouse model. Journal of Controlled Release 2009;134(1):18–25. [PubMed: 19010364]
50. Mai J, Song S, Rui M, Liu D, Ding Q, Peng J, Xu Y. A synthetic peptide mediated active targeting of cisplatin liposomes to Tie2 expressing cells. Journal of Controlled Release 2009;139(3):174–181. [PubMed: 19576253]

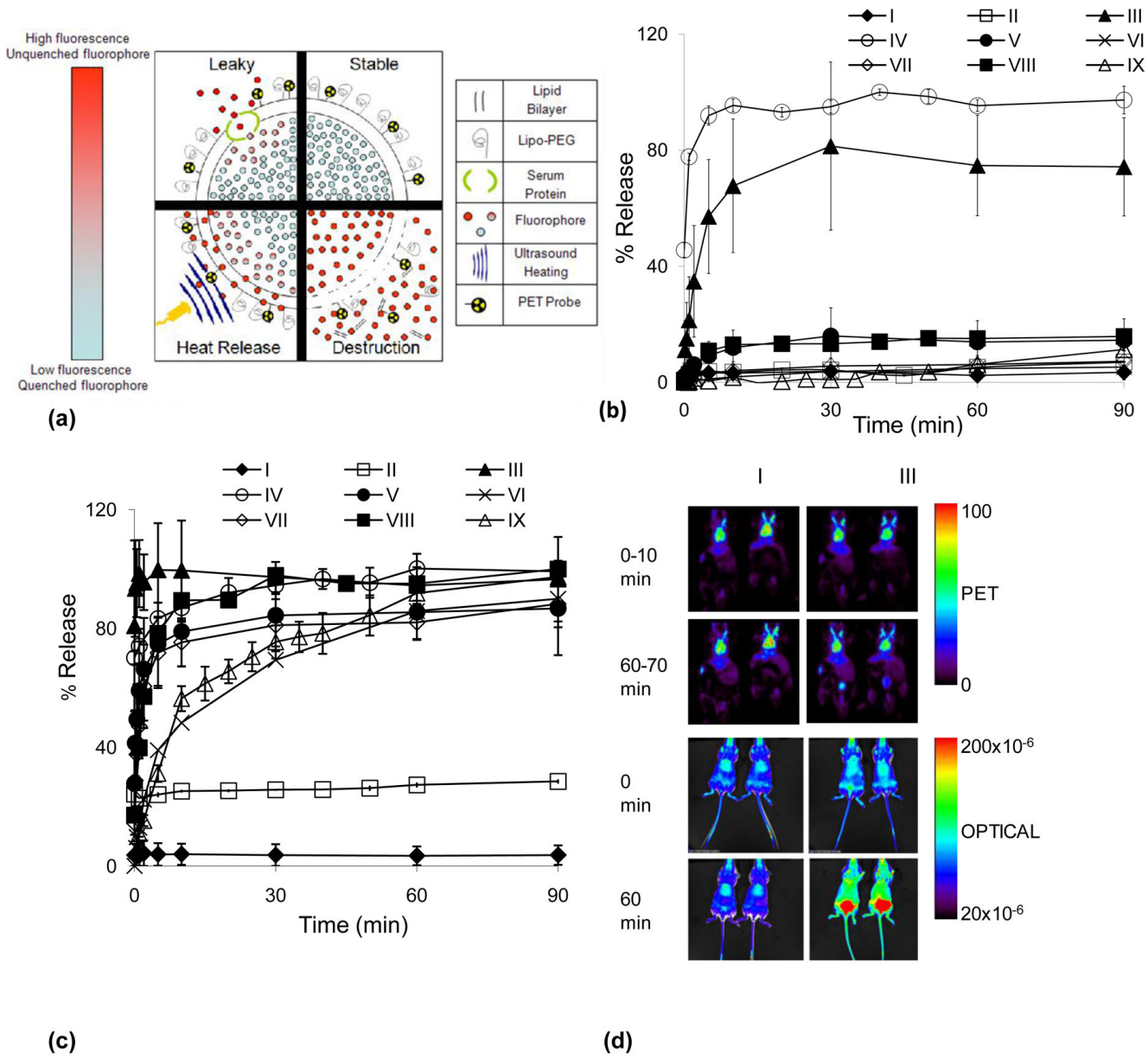

Fig. 1.

Overview of approach. 1a) Illustration of the various mechanisms of liposome fluorophore de-quenching. *Stable*- unchanging low fluorescence of concentrated fluorophore in liposomal core (ex. formulation I). *Leaky*- gradual increase in fluorescence caused by fluorophore leaking through an intact lipid bilayer, often facilitated by serum proteins (ex. formulation V). *Heat Release*- an increase in fluorescence due to applied heat at a rate dependent on liposome temperature sensitivity, ranging from complete de-quenching in seconds (formulations III and IV) to minutes (formulations VI and IX). *Destruction*- immediate increase in fluorescence due to the breakdown of the lipid bilayer, often mediated by lysosomes. 1b) *In vitro* stability assay of formulations I–IX incubated in mouse serum for 90 minutes at 37°C, fluorophore release profiles shown. 1c) *In vitro* temperature response assay of formulations I–IX incubated in mouse serum for 90 minutes at 42°C, release profiles shown. 1d) Sample PET and optical

images of Formulations I and III immediately post intravenous injection and 60 minutes after injection.

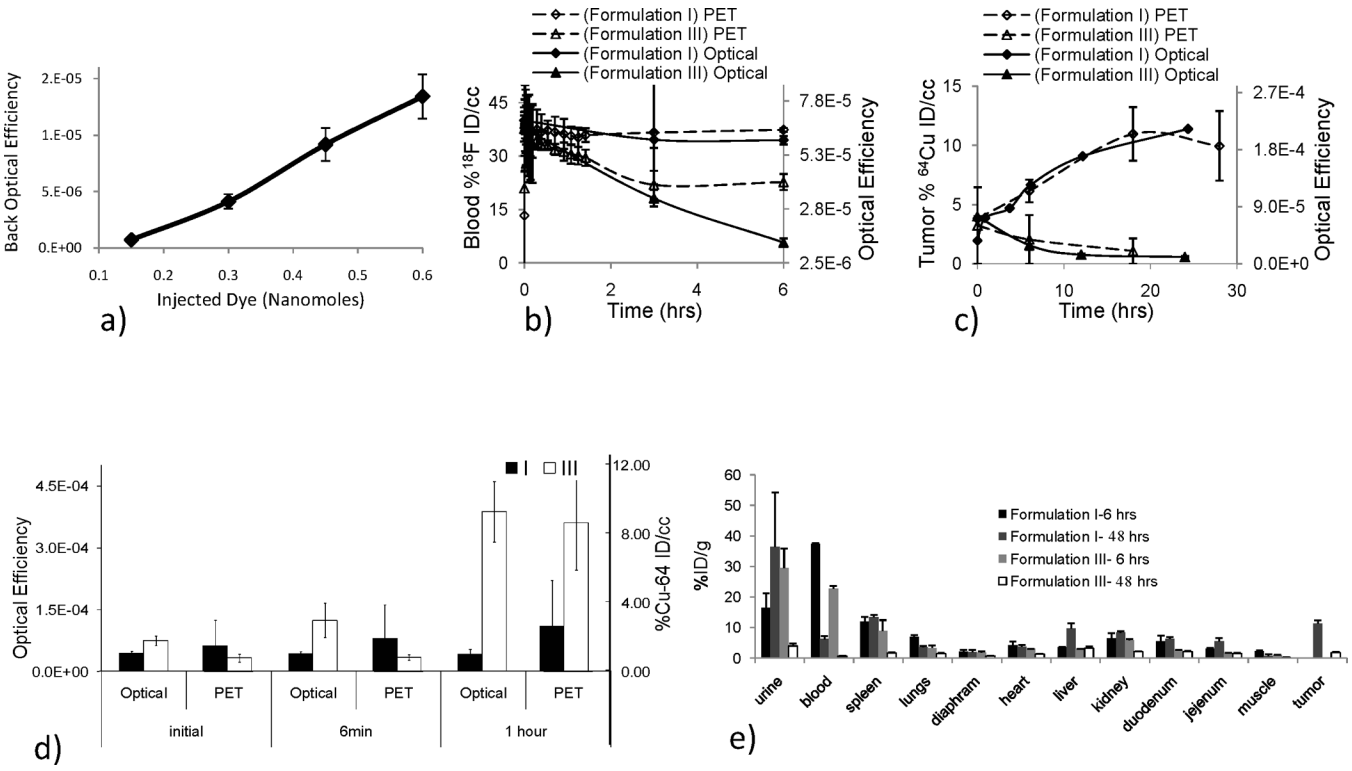

Fig. 2.

Combining PET and optical imaging as a tool for monitoring *in vivo* biodistribution of the liposome shell and core; PET tracks the shell while the optical probe tracks the aqueous core. 2a) *In vivo* optical efficiency resulting from injection of a serial dilution of liposomes ranging from 45 to 180 μg lipid and 0.15 to 0.6 nMols AF-750 verifies the linearity of *in vivo* fluorescence efficiency as a function of fluorophore concentration in the blood pool. 2b) Blood pool radioisotope % ID/cc, using an F-18 labeled lipid as a PET tracer, and optical efficiency vs time. Formulation I shows similar blood pool kinetics when monitoring the shell and core through both PET and optical methods, respectively. However, blood pool fluorescence of formulation III decreases as compared with radioisotope concentration, presumably through the "leaky" mechanism described in figure 1a. 2c) Tumor radioisotope % ID/cc, using a Cu-64 labeled lipid as a PET tracer of the shell, and optical efficiency of the vehicle core vs time. PET and optical probes of tumor accumulation show similar kinetics for each formulation. PET data in 2c also used within [45]. 2d) Bladder accumulation of the F-18 synthesized lipid as a PET tracer and AF-750 as an optical probe at the time of injection, after 6 min and 1 hour. 2e) Biodistribution of PET probes at 6 and 48 hours after injection using F-18 and Cu-64 labeled lipids as PET tracers, respectively (tumor accumulation not assessed at the 6-hour time point).

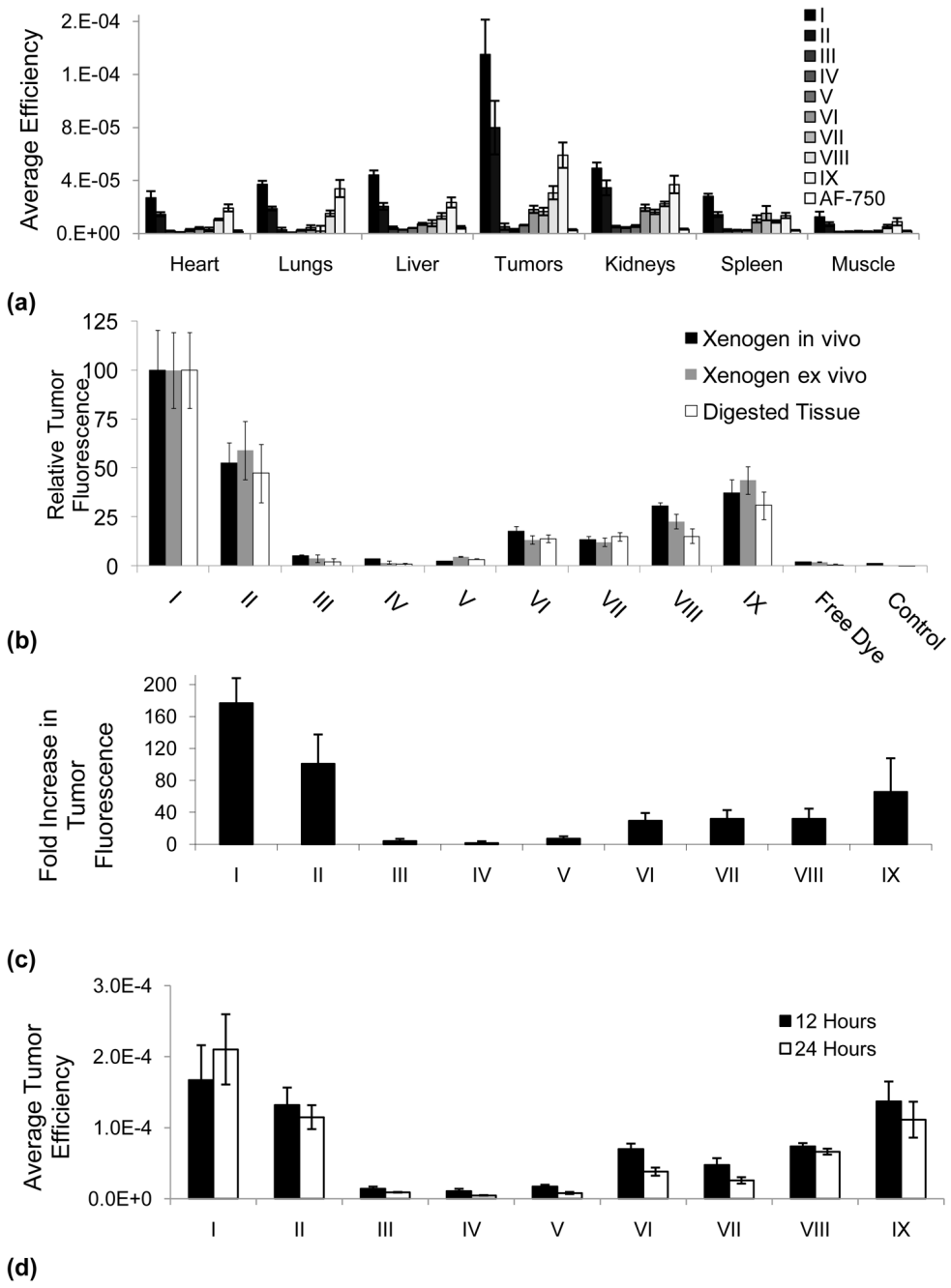

Fig. 3.

Ex vivo and *in vivo* quantitation of fluorescence and efficiency of AF-750 loaded liposomes. 3a) *Ex vivo* quantification of organ fluorescence 24 hours post intravenous injection of AF-750 loaded liposomes. 3b) *In vivo* and *ex vivo* quantification of tumor fluorescence using IVIS imaging system compared with fluorescence of digested tissue measured *ex vivo*. 3c) Quantification of the fold increase in tumor fluorescence for digested, buffered tissue relative to the injection of free AF-750. Stable vehicle accumulation (I) is 177 times greater than free dye; temperature sensitive vehicle (IX and II) accumulation is 66 to 101 times greater than free dye, respectively. 3d) Changes in tumor fluorescence from 12 to 24 hours for formulations I–IX.

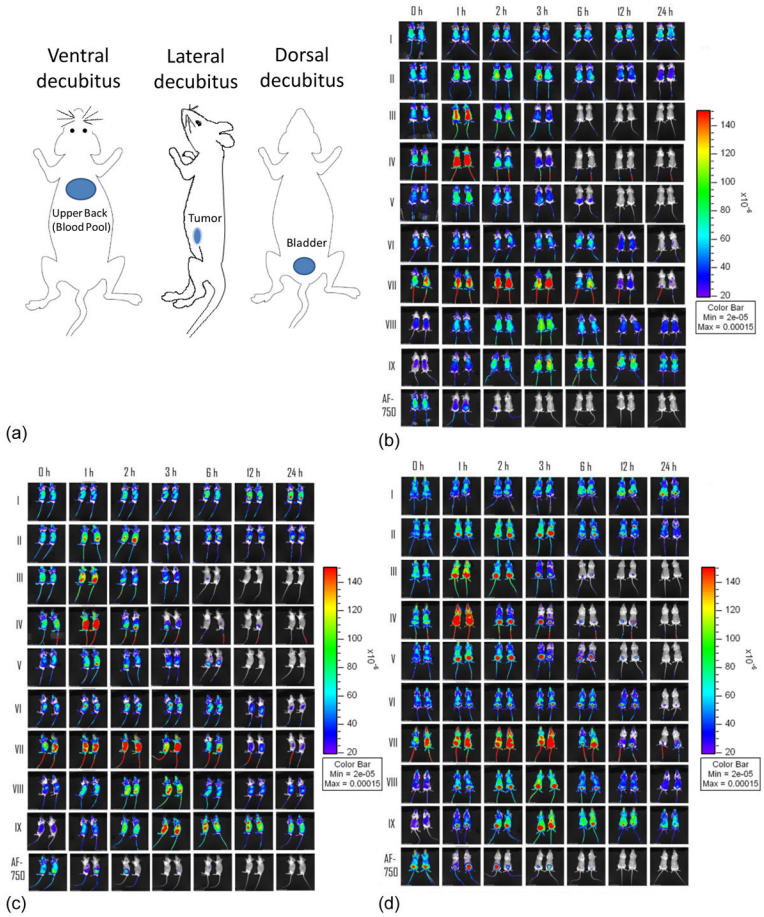

Fig. 4.

In vivo fluorescence imaging of FVB mice bearing bilateral Met-1 tumors over 24 hours after injection of liposomes containing matched lipid and fluorophore concentration for nine formations. 4a) Cartoon schematic of ROI locations, 4b) Ventral decubitus, 4c) Lateral decubitus, 4d) Dorsal decubitus.

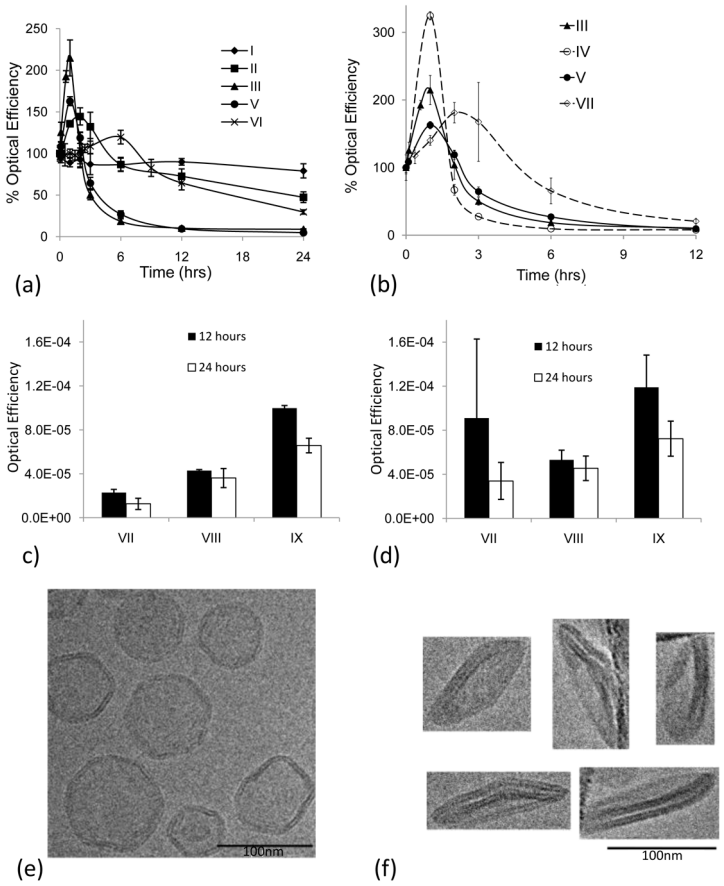

Fig. 5.

5a–d. Optical image efficiency of superficial tissue following injection of AF-750 loaded liposomes, normalized by initial fluorescence for each formulation. 5a) Optical efficiency of superficial tissue (as an indicator of blood concentration and stability) after injection of isotonic liposomes containing negatively-charged lipid-PEG moieties. Longest circulation for high cholesterol and HSPC (I and II); shortest for lysolipid and DPPC (III, IV). Two temperature sensitive formulations (II and VI) demonstrate extended circulation. 5b) Optical efficiency of superficial tissue (as an indicator of blood concentration and stability) after injection of temperature-sensitive formulations containing uncharged lipopolymer (Ceramide-PEG2k) and negatively-charged lipopolymer (DSPE-PEG2k) (III vs IV and V vs VII). 5c) Optical efficiency of superficial tissue (as an indicator of blood concentration and stability) after injection of iso-osmolar (300 mOsm (VII)) and hypo-osmolar (38 mOsm (VIII) and 10 mOsm (IX) liposomes). Decreased osmolarity increases duration of fluorescence. 5d) Optical efficiency of bladder (as an indicator of particle stability). Decreasing the osmolarity of the entrapped AF-750 solution increases fluorophore retention, as shown by prolonged fluorophore clearance to the bladder. 5e–5f. TEM imaging of DPPC:DSPC:Ceramide-PEG2k (85.5/9.5/5 molar ratio) liposomes at room temperature in 300 mOsm PBS. 5e) Isotonic liposomes prepared in 300 mOsm PBS; angular spherical vesicles are produced due to the high gel-to-liquid-crystalline phase transition temperatures of the liposome membranes (>42°C). 5f) Hypotonic liposomes prepared in 10 mOsm PBS yield flat, circular disk-like vesicles.

Table 1

Liposome compositions

Liposome #	Lipid formulation (Short description)	Composition (molar ratios)	Size (nm)	Osmolarity (mOsm)	References
I	SoyPC:Chol:DSPE-PEG2k **(High cholesterol/long circulating)**	56:39:5	91 ±24	300	[37]
II	DPPC:SoyPC:Chol:DSPE-PEG2k **(Temperature sensitive/long circulating)**	54:27:16:3	99 ±8	300	[38]
III	DPPC:lyso-PalmitoylPC:DSPE-PEG2k **(Lysolipid temperature sensitive)**	86:10:4	95 ±25	300	[39]
IV	DPPC:lyso-PalmitoylPC:Ceramide-PEG2k **(Ceramide-PEG version of III)**	86:10:4	101 ±22	300	[39,40]
V	DPPC:DSPC:DSPE-PEG2k **(Classical temperature sensitive)**	85.5:9.5:5	80 ±21	300	[41]
VI	DPPC:DSPC:Comb-PEG **(Comb-PEG version of V)**	89.1:9.9:1	113 ±27	300	[41,42]
VII, VIII, IX	DPPC:DSPC:Ceramide-PEG2k **(Ceramide-PEG versions of V with varied osmolarity)**	85.5:9.5:5	99 ±14, 94 ±17, 92 ±20	300, 38, 10	[40,41]